Volume-1, Issue-2

SREEPATHY

JOURNAL OF ELECTRICAL AND ELECTRONICS ENGINEERING

Published by

Department of Electrical and Electronics Engineering

Sreepathy Institute of Management and Technology, Vavanoor

Palakkad - 679 533

January 2015

Contents

LIGHTNING PHENOMENA

Prof. Thankachen P.V
Head Of Department
Department of Electrical and Electronics Engineering ,
Sreepathy Institute of Management & Technology, Vavannoor, Palakkad, India-679533
E-mail: thankachen.pv@simat.ac.in

***Abstract*— This paper explains about the lightning phenomenon.Lightning is a powerful sudden flow of electricity (an electrostatic discharge) accompanied by thunder. Lightning is an electric discharge in the form of a spark or flash originating in a charged cloud. It has now been known for a long time that thunder clouds are charged, and that the negative charge centre is located in the lower part of the cloud where the temperature is about - 50C, and that the main positive charge centre is located several kilometres higher up, where the temperature is usually below - 200C. In the majority of storm clouds, there is also a localised positively charged region near the base of the cloud where the temperature is 0C.**

***Keywords*—Natural Language Generation (NLG), Karaka Relations, Knowledge Representation.**

I. MECHANISM OF LIGHTNING

Lightning is an electric discharge in the form of a spark or flash originating in a charged cloud. It has now been known for a long time that thunder clouds are charged, and that the negative charge centre is located in the lower part of the cloud where the temperature is about - 50C, and that the main positive charge centre is located several kilometres higher up, where the temperature is usually below - 200C. In the majority of storm clouds, there is also a localised positively charged region near the base of the cloud where the temperature is $0^0 C$.

Fields of about 1000 V/m exist near the centre of a single bipolar cloud in which charges of about 20 C are separated by distances of about 3 km, and indicate the total potential difference between the main charge centres to be between 100 and 1000 MV. The energy dissipated in a lightning flash is therefore of the order of 1000 to 10,000 MJ, much of which is spent in heating up a narrow air column surrounding the discharge, the temperature rising to about 15,000 0C in a few tens of microseconds. Vertical separation of the positive and negative charge centres is about 2 - 5 km, and the charges involved are 10 - 30 C. The average current dissipated by lightning is of the order of kilo-amperes. During an average lightning storm, a total of the order of kilo-coulombs of charge would be generated, between the 00C and the -40 0C levels, in a volume of about 50 km^3.

II. BREAKDOWN PROCESS

Under the influence of sufficiently strong fields, large water drops become elongated in the direction of the field and become unstable, and streamers develop at their ends with the onset of corona discharges. Drops of radius 2 mm develop streamers in fields exceeding a 9 kV/cm - much less than the 30 kV/cm required to initiate the breakdown of dry air. The high field need only be very localised, because a streamer starting from one drop may propagate itself from drop to drop under a much weaker field.

When the electric field in the vicinity of one of the negative charge centres builds up to the critical value (about 10 kV/cm), an ionised channel (or streamer) is formed, which propagates from the cloud to earth with a velocity that might be as high as one-tenth the speed of light.

Usually this streamer is extinguished when only a short distance from the cloud. Forty micro-seconds or so after the first streamer, a second streamer occurs, closely following the path of the first, and propagating the ionised channel a little further before it is also spent. This process continues a number of times, each step increasing the channel length by 10 to 200m. Because of the step like sequence in which this streamer travels to earth, this process is termed the stepped leader stroke. When eventually the stepped leader has approached to within 15 to 50 m of the earth, the field intensity at earth is sufficient for an upward streamer to develop and bridge the remaining gap. A large neutralising current flows along the ionised path, produced by the stepped leader, to neutralise the charge. This current flow is termed the return stroke and may carry currents as high as 200 kA, although the average current is about 20 kA.

The luminescence of the stepped leader decreases towards the cloud and in one instances it appears to vanish some distance below the cloud. This would suggest that the current is confined to the stepped leader itself. Following the first, or main stroke and after about 40 ms, a second leader stroke propagates to earth in a continuous and rapid manner and again a return stroke follows. This second and subsequent leader strokes which travel along the already energised channel are termed dart leaders.

What appears as a single flash of lightning usually consist of a number of successive strokes, following the same track in space, at intervals of a few hundredths of a second. The average number of strokes in a multiple stroke is four, but as many as 40 have been reported. The time interval between strokes ranges from 20 to 700 ms, but is most frequently 40-50 ms. The average duration of a complete flash being about 250 ms.

The approximate time durations of the various components of a lightning stroke are summarised as follows.

Stepped leader = 10 ms
Return stroke = 40 V
period between strokes = 40 ms
duration of dart leader = 1 ms

For the purpose of surge calculations, it is only the heavy current flow during the return stroke that is of importance. During this period it has been found that the waveform can be represented by a double exponential of the form
$i = I(e^{-t}e^{t})$
with wavefront times of 0.5 - 10 s, and wavetail times of 30 200 s (An average lightning current waveform would have a wavefront of the order of 6 s and a wavetail of the order of 25 μ s.)

The standard voltage waveform used in high voltage testing has a 1.2 / 50 μs waveform to take into accound the most severe conditions. For the standard waveform, the coefficients and β in the double exponential have values of $\alpha = 1.426x10^4 s^{-1}, and = 4.877x10^6 s^{-1}$

III. FREQUENCY OF OCCURRENCE OF LIGHTNING FLASHES

A knowledge of the frequency of occurrence of lightning strokes is of utmost importance in the design of protection against lightning. The frequency of occurrence is defined as the flashes occurring per unit area per year.

However, this cannot be measured very easily, and without very sophisticated equipment. This information is difficult to obtain. However, the keraunic level at any location can be quite easily determined. The keraunic level is defined as the number of days in the year on which thunder is heard. It does not even distinguish between whether lightning was heard only once during the day or whether there was a long thunderstorm. Fortunately, it has been found by experience that the keraunic level is linearly related to the number of flashes per unit area per year. In fact it happens to be about twice the number of flashes/square mile/year. By assuming this relationship to hold good throughout the world, it is now possible to obtain the frequency of occurrence of lightning in any given region quite easily.

IV. LIGHTNING PROBLEM FOR TRANSMISSION LINES

The negative charges at the bottom of the cloud induces charges of opposite polarity on the transmission line. These are held in place in the capacitances between the cloud and the line and the line and earth, until the cloud discharges due to a lightning stroke. There are three possible discharge paths that can cause surges on the line.

(a)In the first discharge path (1), which is from the leader core of the lightning stroke to the earth, the capacitance between the leader and earth is discharged promptly, and the capacitances from the leader head to the earth wire and the phase conductor are discharged ultimately by travelling wave action, so that a voltage is developed across the insulator string. This is known as the induced voltage due to a lightning stroke to nearby ground. It is not a significant factor in the lightning performance of systems above about 66 kV, but causes considerable trouble on lower voltage systems.

(b)The second discharge path (2) is between the lightning head and the earth conductor. It discharges the capacitance between these two. The resulting travelling wave comes down the tower and, acting through its effective impedance, raises the potential of the tower top to a point where the difference in voltage across the insulation is sufficient to cause flashover from the tower back to the conductor. This is the so-called back-flashover mode.

(c)The third mode of discharge (3) is between the leader core and the phase conductor. This discharges the capacitance between these two and injects the main discharge current into the phase conductor, so developing a surge- impedance voltage across the insulator string. At relatively low current, the insulation strength is exceeded and the discharge path is completed to earth via the tower. This is the shielding failure or direct stroke to the phase conductor. The protection of structures and equipment from the last mode of discharge by the application of lightning conductors and/or earth wires is one of the oldest aspects of lightning investigations, and continue to do so.

V. SHIELDING BY OVERHEAD GROUND WIRES

Overhead ground wires are provided on transmission lines to intercept direct strokes of lightning and thus keep it off the phase conductor, and to reduce the surge current and hence the overvoltage on a phase conductor by having currents induced in it.

The proportion of lightning flashes capable of causing sparkover of line insulation decreases as the system voltage increases. This is due to the fact that the magnitude of the overvoltage caused by lightning strokes are almost independent of the system voltage. Of course there is a slight dependence as the height of the towers also increase with the increase in voltage and a taller tower is more liable to a lightning strike. For a given magnitude of lightning overvoltage, the per unit value based on system voltage decreases as the system voltage increases. Thus as the system voltage increases, there are lesser number of flashovers caused by lightning.

Not only does the tall tower attract more lightning strokes, but also it requires a much better earth-wire coverage for a given degree of protection.

VI. AREA OF ATTRACTION OF TRANSMISSION SYSTEMS TO LIGHTNING

Protective zone of lightning conductor: The area over which a lightning stroke will be attracted to and will terminate on a lightning conductor in preference to earth is termed the protection range or protective zone. The calculation of the area is based on a gradient of 3 kV/cm at the tower at which the upward streamer is initiated from the tower. It has been found that for the average stroke the protective ratio is approximately two for a lightning conductor or tower.
R = 2 H (approx) at 20 kA

That is, the area of attraction of a lightning conductor may be expected to be equal to an area around the base of the conductor with a radius of twice the conductor height. In the case of transmission lines, the earth wire is positioned to protect the phase conductors against lightning strokes and hence it is a protective conductor. However, the earth wire attracts strokes that would not normally terminate on the line. Similarly, phase-conductors themselves attract lightning strokes and it is hardly correct to talk of the protective zone. A more appropriate term is the area of attraction.

Since the tower is like a lightning conductor, the area of attraction of the tower can be taken as equal to a circle with radius twice the tower height. An earth wire is more uniform that a transmission tower, in that it does not have a sharp point but a sharp line. It has been estimated that an area either side of the earth wire to a distance of 1.5 or 1.6 times the effective height of the earth wire multiplied by the length of the earth wire is a reasonable value to be taken. Further it must be noted that due to the sag of the earth wire, the effective height of the earth wire is itself only about 80% of the height at the tower. Thus a distance of 64% of the radius of attraction at the tower may be taken for the attraction distance of the earth wire. The phase conductor may be treated similarly, but with the height of the phase conductor being considered instead of that of the earth wire. Thus if the line dimensions are known, it is possible to evaluate the total area of attraction that the line has to lightning strokes.

VII. EFFECTS OF LIGHTNING ON A TRANSMISSION LINE

Charged clouds induce charges on upstanding objects. These induced charges are distributed in such a way as to cause a concentration of potential at the upper end of the object, with the result that the electrostatic stress is very great. This causes the air in the immediate neighborhood to be ionised very rapidly, and charged particles are expelled from the pointed end. This produces a gradual lowering of the resistance of the discharge path between the cloud and the conductor until eventually the lightning discharge takes place.

VIII. STROKES TO A PHASE-CONDUCTOR

The charged cloud could discharge directly onto the line. If the line is struck a long distance from a station or substation, the surge will flow along the line in both directions, shattering insulators and sometimes even wrecking poles until all the energy of the surge is spent. If it strikes the line immediately adjacent to a station, then the damage to plant is almost certain, since it is doubtful whether the ordinary lightning arrestor could divert to earth such a powerful discharge, without allowing a part to be transmitted to the terminal apparatus. When lightning strikes an overhead phase-conductor, the magnitude of the current and the high frequency nature of the stroke causes voltage surges to be propagated in both directions from the point of the strike.

The waveshape of these voltage surges is similar to that of the current in the lightning discharge. The discharge current splits itself equally on contact with the phase conductor, giving travelling waves of magnitude e.

$e = Zi(e^{-\alpha t}e^{-betat})$

where Z is the surge impedance of the phase conductor.

Using a typical value for the line surge impedance (say 300 ohm) and an average lighting current (20kA), the voltage waves on the line would have a crest value of

$$E = Zi = (300/2)x20x10^3 = 3MV$$

IX. STROKES TO A TOWER WITH NO EARTH WIRE

Fortunately, direct strokes to the line are infrequent in occurrence compared to side strokes, the effects of which are not so severe. If there is a direct stroke to the tower, a current would be discharged through the metal work of the tower and there would be a potential difference between the top and bottom of the tower.Consider a steel tower having (inductance L) of a transmission line with no earth wire. If the earthing resistance of the tower is R (=5 - 100) and it is struck by lightning, then the potential built up on the tower top would be

R i + L d i /dt

If ei is the induced voltage on the conductor due to the lightning, then the potential difference built up across the tower and the conductor is given by

e = R i + L d i / d t = ei

If the value of e exceeds the line insulation strength, then a flashover occurs from the tower to the line and this is termed a backflashover.

X. STROKES TO EARTH WIRE

When a lightning stroke terminates on the tower of a transmission line having an overrunning earth wire, or terminates on the earth wire of the transmission line, then the resulting current flow and the voltage waves produced by the current iw flowing along the earth wire will travel along the earth wire in both directions from the tower struck. On reaching the neighboring towers they will be partly reflected, and the reflected waves will arrive back at the tower after twice the transit time between the towers. Further reflections will take place as the waves travel further along the earth wire and reaches other towers. In calculation of the resulting voltage wave and hence the potential difference across the insulation it is useful to consider the initial period, first reflection period, second reflection period and so on and obtain separate equivalents.

When the actual tower being struck, the earth wire is struck somewhere near mid-span, then this can be regarded as two towers in parallel being struck for the second reflection period, with the impedance of the span struck acting as an extension to the lightning channel.

For a given tower footing resistance R, strokes to the tower generally develop about one-and-half times the potential at the top of the tower as compared with the strokes to mid span. For a typical lightning current of 20 kA and a tower footing resistance of 20 kA and a tower footing resistance of 20 Ohm, those struck at the tower develop voltages of the order of 200 kV.

XI. STROKES TO NEARBY OBJECTS (INDIRECT STROKES)

These charges are bound (held in that portion of the line nearest to the cloud) so long as the cloud remains near without discharging its electricity by a lightning stroke to an object. If however, the cloud is suddenly discharged, as it is when lightning strikes some object nearby, the induced charges are no longer bound, but travel with nearly the velocity of light, along the line to equalise the potential at all points of the line. This bound charge collapse leads to a voltage wave to be generated on the line in either direction. The value of this is given by

$e_i = ExC2/(C1 + C2) = q/C$
where q = bound charge per unit length of line

C = capacitance per unit length of line

This potential will vary along the line depending upon the distance of each element of line from the lightning stroke.

A Study of Super Capacitor Based Mobile Charging Units in Isolated Power Systems and Automobile Applications

Dileepan V M

Asst. Prof, Dept of Electrical & Electronics Engineering, SIMAT, Vavanoor,

email id: dileepan.vm@simat.ac.in

***Abstract*-Super capacitors or super capacitors are special type of capacitors which have a high charge storage capacity than ordinary capacitors. It is a double layer capacitor (EDLC) used for high values of energy storage. Mobile charging units consists of generator, excitation system, transformer, storage batteries to provide energy to stand-alone /isolated power systems for medical and automobile applications. Super capacitor could store a large amount of charge for a long period of time. So it can be used for standalone isolated power systems. Solar power can be also incorporated with this unit for better performance. This will make the energy storage system more efficient, reliable and also the power factor can be improved. This method can also be used for reactive power compensation in FACTs controllers.**

Key Words-Super Capacitor, isolated/stand-alone power systems, FACTs, energy storage, mobile charging units

I. INTRODUCTION

Super capacitor is a high efficient energy storage capacitor which can store large amount of charge within short periods of time. Super capacitor or super capacitor can be used to store energy in standalone power systems. This paper introduces a simplified model of Super capacitor using constant current charging method. The detailed test procedure for 100 farad super capacitor and ordinary capacitor is analyzed.

II. BASIC DESIGN

Electrochemical capacitors (super capacitors) are a two electrode capacitor separated by an ion permeable membrane (separator) and an electrolyte electrically connecting both electrodes. When the electrodes are polarized with an applied voltage, ions in the electrolyte form electric double layers of opposite polarity to the electrode's polarity which means positively polarized electrodes will have a layer of negative ions form at the electrode/electrolyte interface along with a charge balancing layer of positive ions adsorbing onto the negative layer. The opposite is true for the negatively polarized electrode.

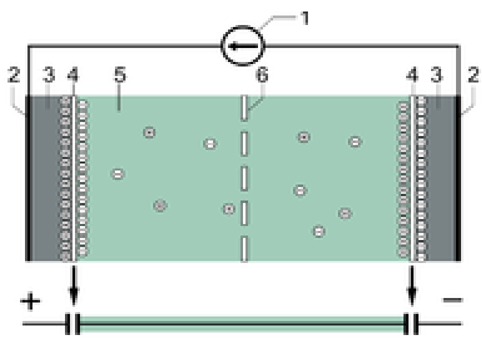

Fig 1. Typical Construction of super capacitor

As there are two layers the effective capacitance is

$$Ctotal = \frac{C1*C2}{C1+C2} \qquad (1)$$

If capacitance values are equal then $C_{total}=0.5C_1$.The capacitances may be symmetric or asymmetric according to the length of parallel plate. If the electrolyte solvent is water then the influence of the high field strength creates permittivity ε of 6 (instead of 80 without an applied electric field) as activated carbon electrodes have a large surface area in the range of 10 to 40 $\mu F/cm^2$ and the extremely thin double layer distance is on the order of a few angstroms (0.3-0.8nm), the double layer capacitors have higher capacitance values than conventional capacitors.

III. STAND ALONE POWER SYSTEMS

Stand alone power systems are used in hospitals, flood affected areas and also in rural areas in which grid connectivity is very difficult. Stand alone power systems consist of a generator, dc excitation system, capacitor bank, storage batteries and transformer.(shown in Fig 2.(a) & (b).

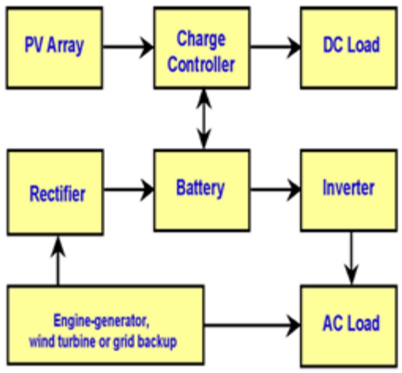

Fig .2(a). Stand alone power system block diagram

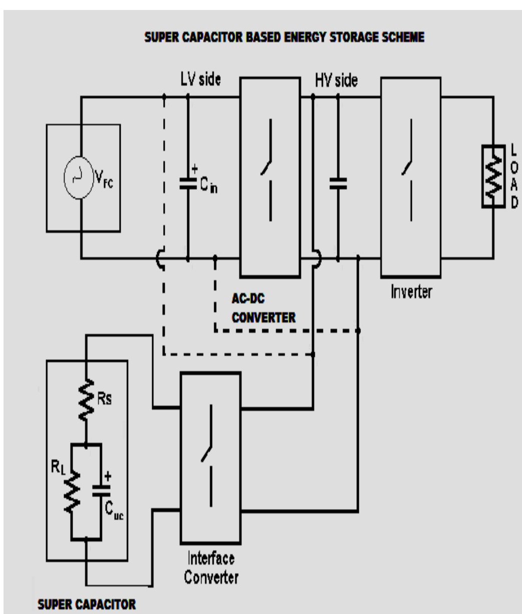

Fig 2.(b).Stand alone power system block diagram

The generator will generate electricity which is rectified and stored using storage batteries. DC link capacitor for stabilizing the voltage is a super capacitor. A super capacitor has several times capacity of an ordinary capacitor and can store more energy. This specialty of super capacitor is utilized in mobile charging units/stand alone power systems

A. Block Diagram

Generator may be of diesel generator (dc excitation) or solar cell or wind turbine generator. It will produce the power needed for the system.

B. Dual converter/ (Rectifier /Inverter)

It will convert AC-DC for storage and then DC-AC after the conversion. The capacitor used as dc link is a super capacitor which is described above.

C. Storage battery

Storage battery may be fuel cell or Li-ion cells or Lead acid accumulator according to the need of the system.

D. Design of Stand Alone /Mobile charging unit.

The load to be fed determines the rating of generator, super capacitor and converter. Suppose the load is 10 KW at 0.9 pf, then the rating of generator is 1.5 k VA. The capacitor will be of 1.5 kV and power converter must be the same voltage and power. This can be also be designed by using a solar cell or wind turbine. This system will give uninterrupted power supply.

IV. EQUIVALENT CIRCUIT OF SUPER CAPACITOR

Fig 3.shows equivalent circuit of super capacitor which consists of R& C combination with a controlled current source. The charge can be controlled by varying the distance between parallel plates. Super capacitor stores more charges than ordinary capacitor or storage battery.

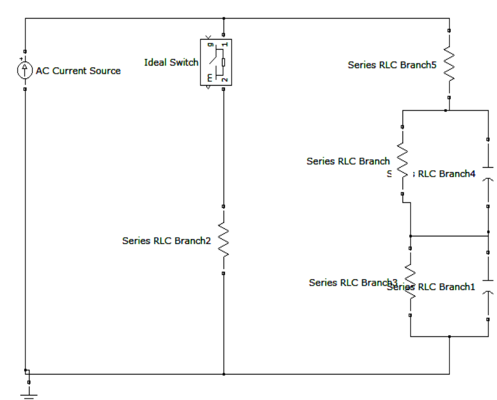

Fig .3.Equivalent circuit of super capacitor

A. Simulation of super capacitor based storage system

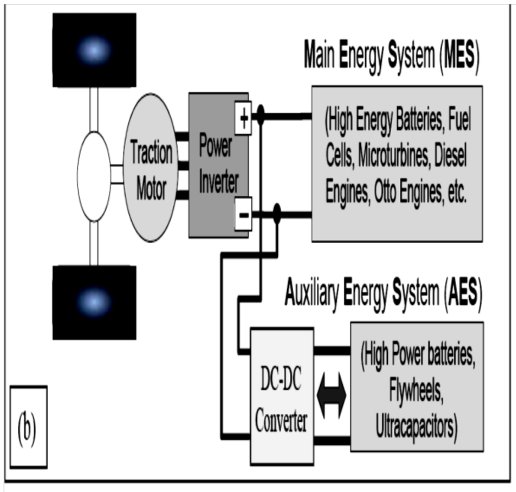

Fig. 4. Block diagram of super capacitor based automobile control system

Fig 3. shows the application of super capacitor based energy storage in automobile traction. The energy can be stored to charge the automobile braking/starting system and also in electric or hybrid vehicle.

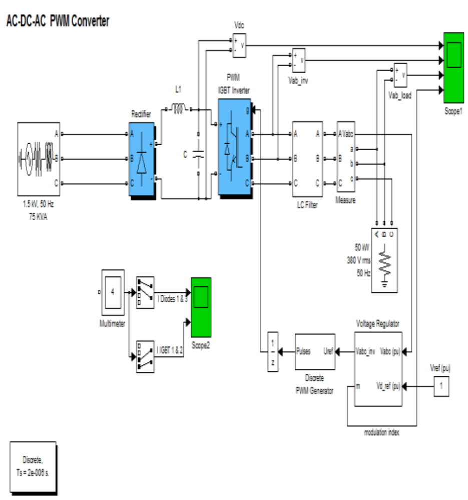

Fig. 5. Simulation diagram of super capacitor based stand-alone power system

Fig 5.Shows the Simulation diagram of super capacitor based stand-alone power system. Simulation diagram consists of a generator connected to a resistive load through a dual converter.The converter is swiched by PWM modulation method.The super capacitor will enhance the capacity to stabilise the voltage.

B. Simulation parameters

Operating Voltage=1.5 K V
Current= 50 A
Power Rating= 75 K VA
Capacitor Rating=1.5 K V;5000µF
Load= 1.1 K W
Converter= Dual Converter
Modulation= Pulse Width Modulation

V. RESULTS

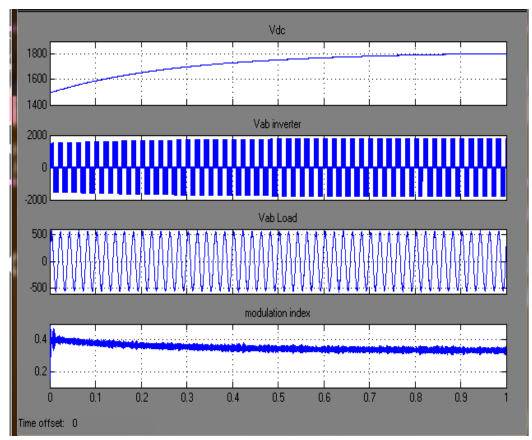

Fig. 6. Simulation results of super capacitor based stand-alone power system

The above Fig. shows the simulation results of a super capacitor based power stabilisation scheme. It is shown in the results that the output power is stablised by a capacitor.The stand alone power system will deliver constant power ,constant voltage,accordng to the need of the load consumed.

VI. ADVANTAGES

- Extends battery run time
- Provides backup power
- Enables design to meet current specifications
- Cuts pulse current noise
- Lessens RF noise by eliminating DC/DC
- Allows low/high temperature operation

- Minimizes space requirements
- Reduces battery size
- Enhances load balancing when used in parallel with a battery
- Meets environmental standards

A. *Engineering Characteristics Super Capacitor*

Charge/Discharge Time	Milliseconds to seconds
Operating Temperature	C -40 ° to +75 °
Operating Voltage Aqueous	1.1 V; Organic 2.5 V
Capacitance	100 mF to > 1000 F
Life	3,000 to 50,000 hrs
Power Density	0.01 to 10 3 kW/kg
Energy Density	0.05 to 10 Wh/kg
Pulse Load	0.1 to 100 A
Pollution Potential	Aqueous electrolyte is highly corrosive

VII. APPLICATIONS

Super capacitors find a wide range of applications such as electric vehicles,hybrid vehicles,stand alone power suppy stem,uninterrupted power systems,medical application including make shift hospitals.

VIII. CONCLUSION

The super capacitor based standalone power systems/mobile charging units are helpful for better storage capacity,uninterrupted power supply,high efficiency,high power factor and less reactive power loss.

IX. FUTURE WORK

The study of super capacitor based power systems, power factor improvement,FACTs controllers, and their real time hardware control module and its installation in residential and industries etc must be done with thorough research ,analysis and simulation.

REFERENCES

[1] A.S. Samosir and A. H. M. Yatim "Dynamic Evolution Control of Bidirectional DC-DC Converter for Interfacing Ultra capacitor Energy Storage to Fuel Cell Electric Vehicle System"2008 Australasian Universities Power Engineering Conference (AUPEC'08). Paper P-113. page 1

[2] Benyahia N.a,*, Denoun H.a, Zaouia M.a, Tamalouzt S.b, Bouheraoua M.a,Benamrouche N.a, Rekioua T.b, Haddad S.a "Characterization and Control of Supercapacitors Bank for Stand-Alone Photovoltaic Energy" Energy Procedia. Sciverse Science Direct 00 (2013)00-00.

[3]Andrew C. Baisden, Student Member, IEEE, and Ali Emadi, Senior Member, IEEE "ADVISOR-Based Model of a Battery and an Ultra-Capacitor Energy Source for Hybrid Electric Vehicles" IEEE Transactions on Vehicular Technology, vol. 53, no. 1, January 2004

[4] M.G. Molina ,P.E. Mercado, " Modeling Of a D-STATCOM With Ultra-Capacitor Energy Storage For Power Distribution System Applications" XIII ERIACDÉCIMO TERCER ENCUENTRO REGIONAL IBERO AMERICANO DE CIGRÉ 24 al 28 de mayo de 2009

BIOGRAPHY

Mr.Dileepan VM was born in June 1985 Shoranur,Palakkad,Kerala,India.He completed his graduation in Electrical & Electronics Engineering from Jyothi Engineeerimng College,Cheruthuruthy,University of Calicut in 2007.Then he worked as Lecturer in Al-Ameen Engineering College,Kulappully,Shoranur,Kerala for one year.Then he completed his ME Course in Power Electronics & Drives from BIT college ,Sathyamangalam,Erode,Tamilnadu, India in 2008-2010.He published two papers on Matrix Converter Based Wind Energy Conversion Scheme in Two National Conferences in 2010.Currently he is working as Assistant Professor in EEE Dept in SIMAT Engg College,Vavanoor, Koottanad,Palakkad,Kerala,India since June 2010.He has published a paper On Thin Film Solar Cell Based Energy Storage System For Vehicles in June 2014.

Image Processing Based Attendance Marking System

Smrithy.K.M
Assistant Professor
smrithykm@yahoo.com
Department of Electrical & Electronics Engineering
Sreepathy Institute of Management and Technology, Vavanoor, Palakkad

***Abstract*- The daily attendance management is a big task in any organization. The image processing based attendance marking system takes the daily attendance of people in industries and educational institutions automatically. The work presented in this paper proposes a method to automatically take the attendance of students in a university. The system makes use of face recognition technology for identifying the students who are present in each class. It is an efficient way to record and manage the attendance activity in a university. The system stores the details of each student as well as their facial features in the database and it compares the new patterns with the previously stored patterns as per the requirement. The system is technologically very simple, easily installable and maintainable. In this paper, one application of the automatic face recognition, such as attendance marking is discussed in detail. Also, the software and hardware details of the system are discussed. The same system with some modifications, can be used in a wide range of applications such as to prove the identity of a person to log in to a computer; to draw cash from an ATM; to identify the presence of known criminals in airports, railway stations, LOC areas in country border etc; to enter a protected site and so on.**

Keywords-Face detection, face recognition, eigen face method, image processing, attendance marking system

I. INTRODUCTION

The conventional personal identification techniques like passwords, keys, barcodes and smartcards have a major drawback: they don't check who is entering or holding the information. They only check whether the correct information is presented to the system. Such systems can be easily deceived because any person who has the ID card or anyone who knows the password can easily claim the identity of that person. Also there are some other drawbacks for such systems: the person has to remember the password or he has to carry the ID card. In barcode system, line of sight reading is required. Biometrics based personal identification systems eliminates most of these drawbacks. Biometrics is the automated recognition of individuals based on their behavioural and biological characteristics. Fingerprint, hand geometry, face, iris scan, retinal scan, signature, gait, voice are some of the well known biometric characteristics. In biometric based attendance systems, subject is being identified using any of biometric techniques Biometric systems are more reliable because biometric characteristics cannot be easily stolen, duplicated or lost and also the user does not have to memorize the password or he does not have to carry some ID cards. But each of these biometric systems has certain disadvantages also. The finger print and hand geometry based systems fail to identify the individuals if the finger or hand is injured or dirty. Retinal and iris scan are very much susceptible to diseases that change the characteristics of the eye. For obtaining the retina scan, laser light must be directed through the cornea of the eye. Iris based systems need a specialized camera which is very expensive and also the photo should be taken very close to the subject. Voice based systems might not work properly if the voice of the person changes due to flu or throat infection. Any noise in the background also affects the performance of the system. So, compared to the above mentioned biometric systems, face recognition based systems have many advantages due to the following reasons:

- Easy to deploy, can use existing image capturing devices (webcam, security camera etc)
- Contact free process
- It does not require user cooperation unlike fingerprint. People can be identified without their knowledge [2].
- It is easier to obtain a photo rather than a finger print or iris scan.

Face recognition systems have numerous applications in access control systems, network security, crowd surveillance systems, and attendance systems and so on. In this paper, the design and implementation of a face recognition system is discussed in detail. And the system performance is evaluated for an application like automatic attendance marking of students in a university. The system identifies the students with the help of image processing technologies. So students who are absent and intruders are checked out automatically. In the proposed system, cameras installed in each class room will capture the photo of the students. Each student will be identified using face recognition technology and the attendance report will be generated automatically. The system can locate a subject's face and then recognize the person by comparing characteristics of the face to those of known individuals. For face recognition, eigen face approach (proposed by M Turk and A Pentland [3, 5, 6]) is used.

The entire paper is organized as described below. Section II presents an overview of image processing technique. Also the algorithms used for implementing face detection and face recognition are discussed. Section III describes the implementation details of image processing based attendance marking system. Results and discussion are given in section IV followed by conclusion in section V.

II. IMAGE PROCESSING

Image processing implies a set of computational techniques for analyzing, enhancing, compressing and reconstructing images. Image processing has extensive applications in many areas, including astronomy, computer vision, robotics, remote sensing by satellites, medical image processing and biometrics. An overview of face recognition system and the algorithms used for implementing the image processing based attendance marking system are described in the coming sections.

A. Outline of face recognition system

The system is made up of a camera which take the photos of individuals and a computer unit which performs face detection (locating faces from the image removing the background information) and face recognition (identifying the persons). First, face images are acquired using webcam to create the database. Face recognition system will detect the location of face in the image and will extract the features from the detected faces. As a result of feature extraction process, templates are generated which is a reduced set of data that represents the unique features of enrolled user's face. These templates are stored in database. For an unknown face image, template is generated as described above and is compared with those stored in the database, which outputs the identity of that face if a match occurs. An overview of face recognition system is shown in fig. 1.

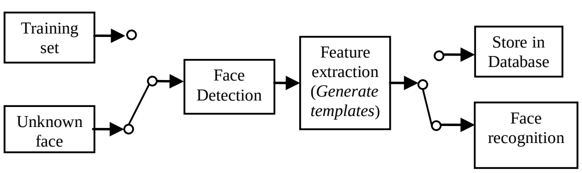

Fig. 1. Face recognition system

B. Face detection

Face detection is the first and the most important step towards face recognition. Given images with different complex backgrounds, a face detection algorithm will identify and locate the faces in the image accurately. In the proposed system, for face detection, an efficient and rank deficient approach proposed by Wlof Kienzle and Gokhan Bakir [4] is used. It is a method for computing fast approximations to support vector decision functions in the field of object detection.

C. Face recognition

A simple approach to extract the information contained in an image of a face is to somehow capture the variation in a collection of face images, independent of any judgement of features, and use this information to encode and compare individual face images [6]. The system functions by projecting face images onto a feature space that spans the significant variations among known face images. The significant features are known as eigenfaces because they are the eigen vectors (principal components) of the set of faces; they do not necessarily correspond to features such as eyes, ears and noses [5]. The projection operation characterizes an individual face by a weighted sum of the eigen face features, and so to recognize a particular face it is necessary only to compare these weights to those of known individuals [7].

Let the training set of M number of face images be $\Gamma_1, \Gamma_2, \ldots, \Gamma_M$, then the average of the set is defined by

$$\Psi = \frac{1}{M}\sum_{n=1}^{M}$$

Each face differs from the average by the vector

$$\Phi_i = \Gamma_i - \Psi$$

This set of very large vectors is then subject to principal component analysis which seeks a set of M orthonormal vectors, U_m, which best describes the distribution of the data. The k^{th} vector ,U_k, is chosen such that

$$\lambda_k = \frac{1}{M}\sum_{n=1}^{M}(U_k^T \Phi_n)^2$$

is a maximum subject to

$$U_l^T U_k = \delta_{lk} = \left\{ \begin{array}{c} 1, \text{ if } l=k \\ 0, \text{ otherwise} \end{array} \right\}$$

The vectors U_k and scalars λ_k are the eigenvectors and eigen values respectively of the covariance matrix

$$C = \frac{1}{M}\sum_{n=1}^{M}\Phi_n \Phi_n^T = AA^T$$

where the matrix $A = [\Phi 1\ \Phi 2 \ldots\ \Phi_M]$. The covariance matrix C is $N^2 * N^2$ and calculating N^2 eigen vectors and eigen values is an intractable task for typical image sizes. So a computationally feasible method is needed.

Consider the eigen vectors v_i of A^TA such that

$$A^TA\, v_i = \mu_i\, v_i$$

Pre multiplying both sides by A, we have

$$AA^TA\, v_i = \mu_i\, Av_i$$

where Av_i are the eigen vectors and μ_i are the eigen values of $C=AA^T$

Following these analysis, we construct the M × M matrix $L=A^TA$, where $L_{mn} = \Phi_m^T \Phi_n$ and find the M eigen vectors, v_i, of L. These vectors determine linear combinations of the M training set face images to form the eigenfaces U_l

$$U_l = \sum_{k=1}^{M} v_{lk}\, \Phi_{k},\ l=1,\ldots,M$$

With this analysis, the calculations are greatly reduced from the order of the number of pixels in the images (N^2) to the order of the number of images in the training set (M). In practice, the training set of face images will be relatively small ($M \ll N^2$). From analysis it is found that M' (M'<M) significant eigen vectors of the L matrix with the largest associated eigen values are sufficient for reliable representation of the faces in the face space characterized by the eigen faces [3].

For new face image (Γ) to be recognized, it is transformed in to its eigen face components (projected onto "face space") by a simple operation,

$w_k=U_k^T (\Gamma - \Psi)$

for k=1,…,M'. The weights form a projection vector,

$$\Omega^T = [w_1\ w_2 \ldots w_{M}]$$

describing the contribution of each eigen face in representing the input face image, treating the eigen faces as a basis set for face images. For the input face image also, calculate the projection vector as described above and compare it with projection vector corresponding to each face stored in the database. The idea is to find the face that minimizes the difference. If the difference is minimum for a particular person's face in the database then, it can be concluded that the input face is of that person

III. IMAGE PROCESSING BASED ATTENDANCE MARKING SYSTEM

The system enables marking the attendance of students in a university by making use of the face recognition technique. First, the students are enrolled in the database with their face images. To mark the attendance, photos of the students who are present in the class are taken using webcam. Based on the photos taken, the system will recognize each student and their attendance will get marked in an excel sheet automatically which can be saved for later use. The software and hardware details of the system are given in the following sections.

A. The image processing based attendance marking system application

The image processing based attendance marking application is developed in MATLAB7.6.0 (R2008a). It does the following tasks

1) Enroll faces (add images to the database)
2) Detect and extract faces from the images added.
3) Create eigenfaces for all the extracted faces and store them in the database.
2) Update database (If needed)
3) Test input images
4) Mark the attendance for the recognized students in an excel sheet automatically.

The flow chart for the entire application is shown in fig. 2. It mainly consists of two subsystems; create database and test faces.

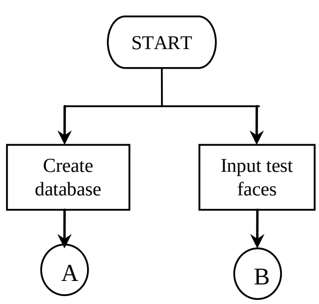

Fig. 2. Flow chart for image processing based attendance marking system application GUI

The front end view of the GUI created is shown in fig. 3.

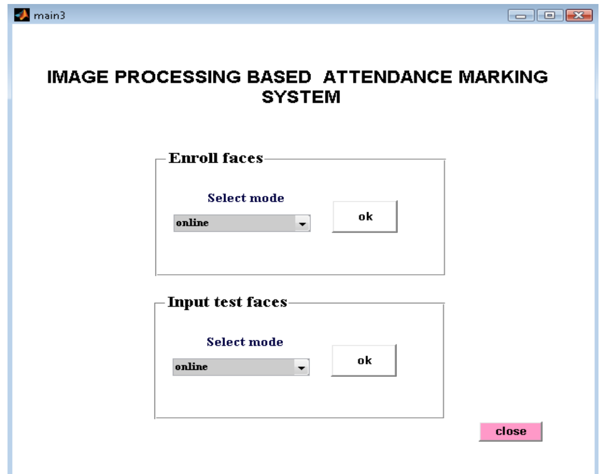

Fig. 3. Front-end view of the GUI for the image processing based attendance marking system application

In the GUI, first the mode for creating the database is to be chosen first. If the photos are taken directly from the camera 'online' option is chosen or if the photos are stored in the system then, 'offline' option is chosen. After selecting the mode to enrol faces in the main window of the GUI, a new window will appear as shown in fig.4. Database creation is done in this window. The flowchart for database creation is shown in fig. 5. After adding all the images to database, eigen faces are calculated.

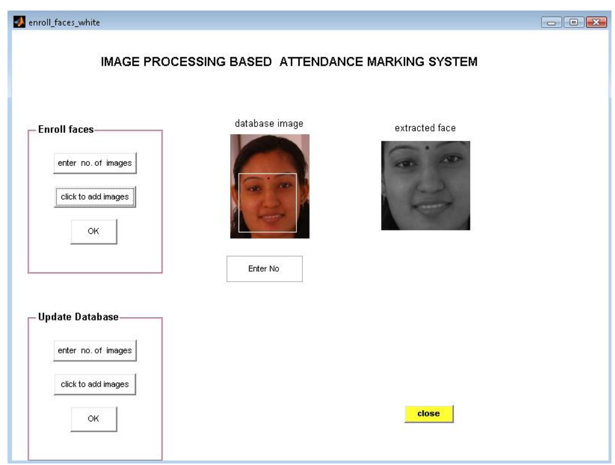

Fig. 4. GUI for enrolling faces in image processing based attendance marking system application

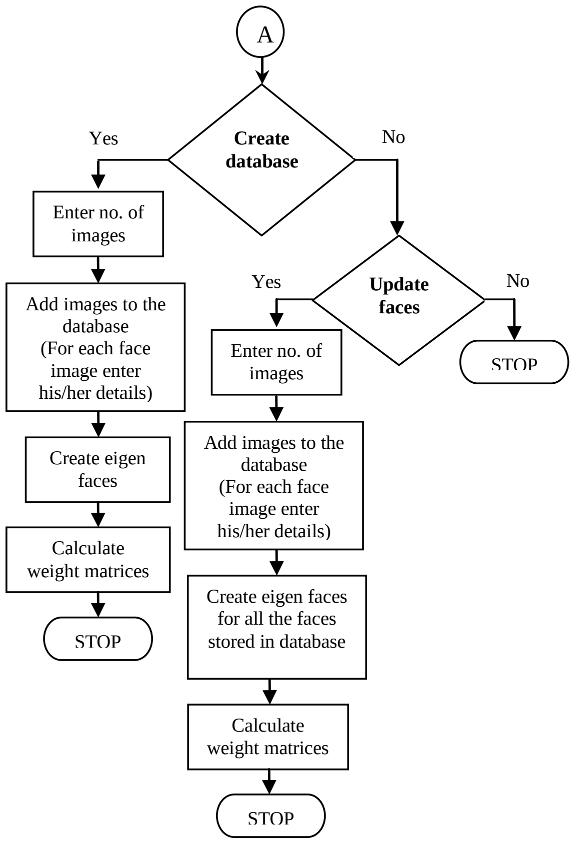

Fig. 5. Flow chart for creating database

Finally 'close' button is pressed to navigate to the main window. In the main window, the mode for inputting the test photos ('offline' or 'online') is chosen. Then a new window for testing the unknown faces will appear as shown in Fig. 6. The flow chart for testing input faces is shown in fig. 7.

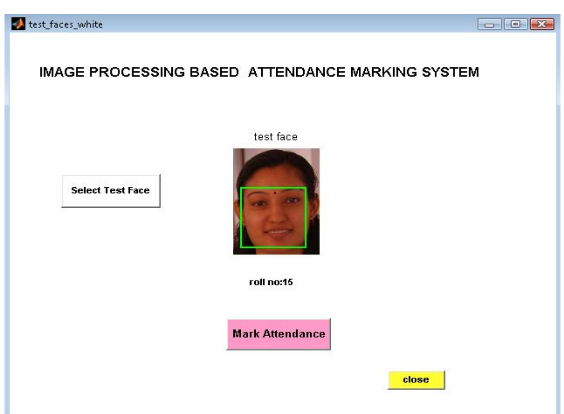

Fig.6. GUI for testing input faces in image processing based attendance marking system application

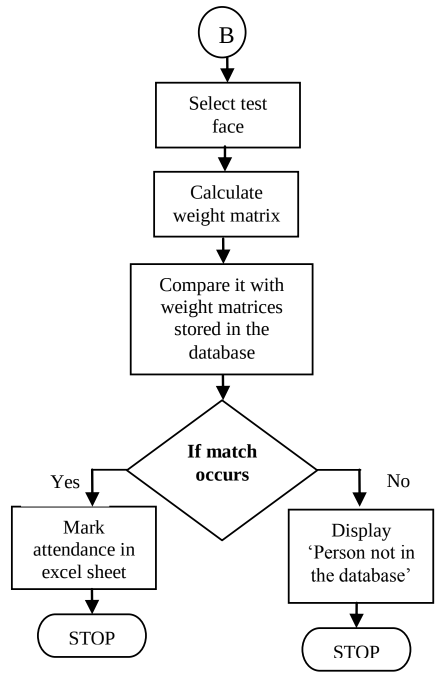

Fig. 7. Flow chart to input test faces

If the mode chosen is 'offline', the 'select test face' option is used, to browse for the test photo. If 'online' selection is made then, the hardware connected to the system will take the photos. Also, the photos will be displayed in the window. Finally, the attendance will get automatically marked in an excel sheet as '1' for the students who are present.

B. The image processing based attendance marking system hardware

The hardware implementation of image processing based attendance marking system was done by making use of a PIC 16F877 micro controller and a Passive Infra Red (PIR) sensor which will detect the presence of a person. The block diagram for the hardware is shown in fig. 8.

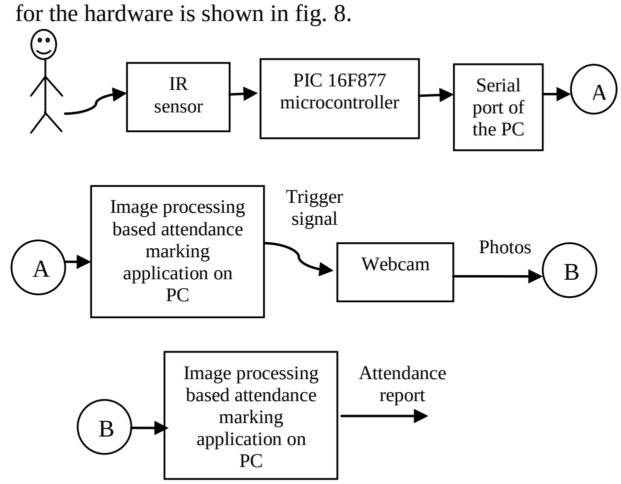

Fig. 8. Hardware block diagram

As soon as the PIR sensor senses the arrival of a person, one pin of the microcontroller goes high which in turn turns on a buzzer and a LED and also transmits a bit ‘1’ serially to the image processing based attendance marking application on PC. If the sensor output is low, bit ‘0’ will be transmitted. Whenever the application detects bit ‘1’, it will turn on the webcam automatically. Then the camera will take the photo and that photo will get processed in the application. Finally the application will generate attendance report.

IV.RESULTS AND DISCUSSION

The application developed in MATLAB for image processing based attendance marking was tested both manually and automatically. First database creation was done using the photos of students in the university. Experiments were carried out using 22 photos. Among them, the face recognition algorithm was able to recognize 15 students correctly. Hence the percentage error obtained was 31.81. The eigen faces calculated are displayed as shown in fig. 9 and the attendance report generated for the students in the university is shown in Fig. 10.

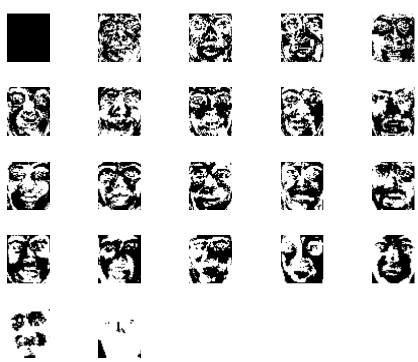

Fig. 9. Eigen faces

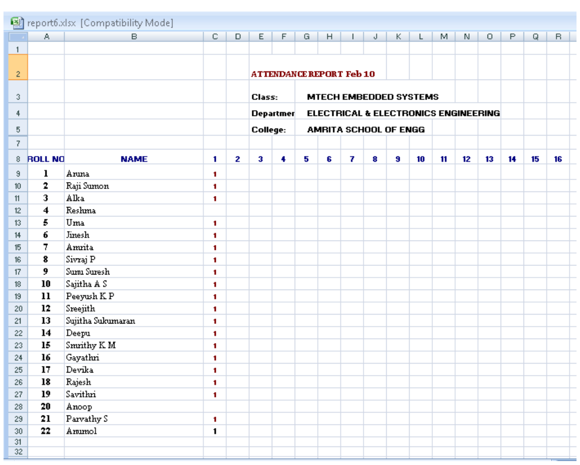

report6.xlsx [Compatibility Mode]

ATTENDANCE REPORT Feb 10

Class: MTECH EMBEDDED SYSTEMS

Departmer ELECTRICAL & ELECTRONICS ENGINEERING

College: AMRITA SCHOOL OF ENGG

ROLL NO	NAME	1	2	3	4	5	6	7	8	9	10	11	12	13	14	15	16
1	Aruna	1															
2	Raji Sumon	1															
3	Alka	1															
4	Reshma																
5	Uma	1															
6	Jinesh	1															
7	Amrita	1															
8	Sivraj P	1															
9	Sunu Suresh	1															
10	Sajitha A S	1															
11	Peeyush K P	1															
12	Sreejith	1															
13	Sujitha Sukumaran	1															
14	Deepu	1															
15	Smrithy K M	1															
16	Gayathri	1															
17	Devika	1															
18	Rajesh	1															
19	Savithri	1															
20	Anoop																
21	Parvathy S	1															
22	Anumol	1															

Fig. 10. Attendance in excel sheet

Usually in the eigen face method, faces are cropped manually to remove the background [2]. But in this proposed system, the objective is to recognize the individuals from a photo automatically. So it was first needed to detect and extract the faces from the photo by using some face detection algorithm and then these extracted faces were to be used for the recognition. As the size of the face extracted by the face detection algorithm was small, there was a high percentage error as above mentioned was experienced in recognizing individuals. Also, there are some more limitations for the eigen face approach. First, the algorithm is sensitive to head scale [8]. Second, it is applicable only to front views. Third, it demonstrates good performance only under controlled background, and may fail in natural scenes. When lighting is highly variable, eigenface often does no better than random guessing would [1, 7, 2]. Other factors that may stretch image variability in directions that tend to blur identity in PCA space include changes in expression, camera angle, head pose, image quality(CCTV, Web-cams etc. are often not good enough) and partial covering (Hats, scarves, glasses)[8].

V.CONCLUSION

In this paper a method for automatic attendance marking in a university has been presented. The system removes some of the drawbacks of traditional attendance system (where the attendance is taken by the teachers manually) like the chances of proxy attendance, wastage of class hours etc. The system can also track the time of entry of each student and it will be written in to the attendance sheet along with their attendance. The above mentioned is one of the applications of the face recognition system which is being developed. The system can be used in a range of applications like PC login security, robotics, vehicle security systems, terrorists screening, passport authentication etc.

REFERENCES

[1] Hetal Patel, “Facial feature extraction for face recognition: a review”, IEEE International Symposium on Information Technology, Vol.2, Aug. 2008

[2] Nicholl, P. Amira, A. , “DWT/PCA Face Recognition using Automatic Coefficient Selection”, 4th IEEE International Symposium on Electronic Design, Test and Applications, Jan. 2008

[3] Kresimir Delac and Mislav Grgic,“Face recognition”, I-TECH Education and Publishing,Vienna,Austria,2007

[4] *Kienzle, W., G. Bakir, M. Franz and B. Schölkopf:* “Face Detection - Efficient and Rank Deficient”, Advances in Neural Information Processing Systems 17, 673-680. (Eds.) Weiss, Y. MIT Press, Cambridge, MA, USA (2005)

[5] Jie Wang, K.N. Plataniotis, A.N. Venetsanopoulos, “Selecting discriminant eigenfaces for face recognition”, Pattern Recognition Letters 26 (2005), science direct

[6] M.Turk. and A.Pentland., “Face recognition using eigenfaces”, Proceedings of IEEE Conference on Computer Vision and Pattern Recognition, Maui, Hawaii, pp. 586-591, 3-6 June 1991.

[7] M. Turk, A. Pentland, “Eigenfaces for Recognition”, Journal of Cognitive Neurosicence, Vol. 3, No. 1, pp. 71-86, 1991

[8] Thomas Heseltine, *“*Evaluation of Image Pre-processing Techniques for Eigenface Based Face Recognition*”* Department of Computer Science, The University of York

Robust Variable Gain Sliding Mode Control of Onshore Container Crane

Smitha G
Department of Electrical Engineering
National Institute of Technology Calicut (NITC)
Kerala, India
smithaghere@gmail.com

Dr. Abraham T Mathew
Department of Electrical Engineering
National Institute of Technology Calicut (NITC)
Kerala, India
atm@nitc.ac.in

***Abstract*—The onshore container cranes are used in the container transshipment terminals of seaports to load and unload containers to and from the container ships. This container crane system is a typical nonlinear under-actuated system with strong states' coupling. While in motion, the trolley translation causes the payload (container) to swing and this is undesirable for many reasons. The objective of the paper is to effectively model the nonlinear container crane system, including the friction and wind disturbance, and to design a Sliding Mode Control (SMC) algorithm based on the non-linear container crane model. The two dimensional 3 Degree of Freedom (3-DOF) model of the container crane system is obtained using Lagrange's equation; friction nonlinearity (Lu-Gre friction model) and wind disturbance are then added to it. In the proposed control law, a sliding surface is designed, which consists of the trolley dynamics, hoisting dynamics and sway angle. A variable control gain is incorporated to reduce the chattering effect of SMC.**

***Index Terms*—Container Transportation; Container Crane; Degree of freedom (DOF); Under-actuated systems; Lagrange's equation; Lu-Gre friction model; Wind load, Sliding mode control (SMC).**

I. INTRODUCTION

Transport of large volume goods is done through sea and the items are packaged in standard size containers for facilitating quick and safe transshipment at various locations and the ultimate transport of the goods to the destinations. Safe handling of containers and the time to load/unload the containers affect the overall work efficiency at the transshipment terminals. The container cranes are the standard equipment used for shifting of containers from land to ship and vice versa. An onshore container crane is a type of large dockside gantry crane, found at the container terminals of seaport, for loading and unloading the containers between container ships and trucks/rail. It has three main parts –a supporting structure called gantry, a trolley that runs on rails and a moving gripper called spreader that locks on to the container by a twist-lock mechanism. The container crane operation consists of three tasks – *container hoisting* from the container ship/truck, *horizontal transportation* between the ship and the truck and *container lowering* to the ship/truck/rail. The overall objective is to speed up the transfer from one place to the next safely and smoothly, albeit the effect of wind, weight or the container size. The performance of the container crane is mainly measured by certain parameters namely- high hoist and trolley speeds resulting in short cycle time, high reliability/availability figures with MTBF (Mean Time between Failures) values of less than 0.5%. Fig 1 shows the onshore container cranes at International Transshipment Terminal (ICTT), Vallarpadam, Kochi, Kerala, India and is included to give a quick idea about the physical arrangements.

Fig 1. Onshore container cranes at International Transhipment Terminal (ICTT), Kochi, Kerala, India [1]

II. CONTROL OBJECTIVES

The main control objective in the container crane operation is to hoist the container with a given pace and track the trolley at the same time so as to reach the destination as fast as possible. This will enable better transportation efficiency; keep the payload swing as small as possible during the transportation process to ensure the safety of the system and the personnel; and to absolutely suppress the container vibrations at the destination so as to enable accurate positioning of the container. Most crane systems in practice are manually operated by experienced workers. Manual operation results in such disadvantages as drudgery and fatigue for the operators, long time delays, long duration training for operators, high operating cost etc. Researchers have identified the need for automatic control systems for mitigating the effects of manual operation and to improve the efficiency and productivity of the transshipment terminals. The main obstacle in achieving good control performance is that the container cranes operate outdoors confronting winds [2]. Robustness in the performance of the crane control systems becomes necessary due to the uncertainties prevailing in the field.

Recently, the automatic control problem for an under-actuated crane system has become a focus of the control community, and many ambitious control laws have been proposed to improve the performance of a container crane. In [3], the input shaping techniques are implemented to reduce the swing of the payload by convolving the human-generated signal with a chosen impulse sequence. This method requires the knowledge regarding the system parameters including natural frequencies and damping ratios. Unfortunately, it often meets great difficulty when trying to obtain these parameters which vary with diverse working conditions such as different rope length. In [4], an open-loop optimal controller is used for overhead crane systems to generate ideal trajectories for the trolley. Besides the previous open-loop control methods, several closed-loop control strategies are often utilized for an overhead crane system to improve control performance. In [5], a series of energy-based controllers is designed to regulate the trolley to a desired position while reducing the swing of the payload at the same time. Since a container crane is a typical under-actuated system, sliding-mode control is often employed to add a control freedom by bringing sliding surfaces into the system [6]. To suppress the oscillation induced by the sliding-mode control, fuzzy logic is introduced into the traditional sliding-mode control methods in [7]. Unfortunately, fuzzy sets and corresponding fuzzy rules are specially hard to tune for a crane system. To achieve satisfactory performance, the trajectory of the trolley is very important. However, due to the under-actuated behavior, the trajectory planning problem for overhead cranes is a very challenging problem [8]. Adaptive SMC control technique for 2 DOF model of container crane and for 3 DOF model of overhead crane are discussed in [9] and [10] respectively. Model reference adaptive control (MRAC) combined with SMC for three dimensional model of overhead crane is detailed in [11].

The objective of the paper is of two fold. Firstly it is proposed to model the nonlinear container crane system, including friction and wind disturbance and secondly a variable gain sliding mode control (SMC) algorithm is proposed based on the non-linear container crane model.

III. METHODOLOGY

It should be pointed out that, when transferring payloads, a container crane is unavoidably affected by various kinds of disturbance, such as the friction between the trolley and the rail, wind load etc. In an automated control setting, these disturbances can cause unpredictable output. So detailed investigation need to be done to study the effect of the uncertainties on the overall performance of the container crane system and also to suggest suitable robust control methods. Hence, the proposed work has adapted ideas from the works reviewed previously and proceeded to include factors such as friction, wind load etc. in the control design. Since sliding mode control is largely proposed for nonlinear control with uncertainties, it has been decided to focus on SMC.

First, a 3 DOF model is obtained using Lagrange's equation; friction nonlinearity (based on LU-GRE friction model) and wind disturbance are then added to it. Sliding mode controller, which is a robust one, is analyzed next by designing a sliding surface consisting of trolley position, rope length and sway angle. To reduce the chattering effect of SMC, a varying control gain is introduced. To demonstrate the efficiency of the proposed algorithm, simulation results are provided.

The remaining part of the paper is organized as follows: Section 4 gives a 3 DOF model of the onshore container crane. In Section 5, sliding mode controller design and the variable gain strategy are discussed. Section 6 gives the simulation results. Conclusions are presented in section 7.

IV. 3 DOF MODEL OF CONTAINER CRANE

Consider the dynamic model of the onshore container crane with variable rope length, illustrated in Fig.4.

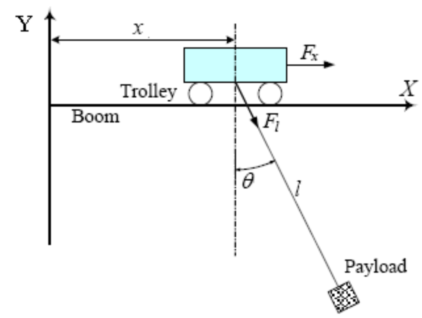

Fig 4. Trolley- cart model of onshore container crane [2]

The container (payload) is picked up by the spreader, both being suspended from the trolley by a rope of length l. The trolley is then moved to the destination carrying the spreader along with the container. On reaching the destination, the container is safely and accurately positioned at the loading point onboard the ship or the stacking point on the shore. Rope length l is variable as the system has to hoist/lower the payload. The masses of the trolley, payload and payload lifting mechanism are m_t, m_p and m_l respectively. f_x is the control force applied to the trolley in the X direction and f_l is the control force applied to the payload in the l direction. Let x be the trolley position along the X-axis, g be the gravitational acceleration and θ be the sway angle. The control forces f_x and f_l are the two inputs. The trolley position x, angular swing of the payload θ and hoist rope length l are the three outputs. The system is under-actuated, as it has fewer control inputs than its degree of freedom.

To start with, the following modeling assumptions are taken: (1) In an actual crane, four ropes are used to hoist the spreader (including the payload). However, for simplicity, only one rope and a point mass is assumed here. (2) It is also assumed that the motions of both the spreader and the rope occur in the vertical plane, that is, the X –Y -plane. (3) Payload is considered as point mass. (4)Rope is assumed to be mass-less, rigid and inflexible. (5) During the overall transferring process, payload is beneath the trolley. (6) All frictional elements in trolley are ignored. (7) Air resistance is ignored. (8) External disturbances like wind are neglected.

Considering the motions of the trolley and the container in the two-dimensional (2D) plane, the co-ordinates of the payload (x_p , y_p) is given by

$$x_p = x + l\sin\theta,\ y_p = -\,l\cos\theta \tag{1}$$

The kinetic energy T of the entire system is given by

$$T = \frac{1}{2}m_t\dot{x}^2 + \frac{1}{2}m_p v_p^2 + \frac{1}{2}m_l\dot{l}^2 \tag{2}$$

where v_p is the velocity of the payload, given by

$$v_p^2 = \dot{x}_p^2 + \dot{y}_p^2 \tag{3}$$

The potential energy U of the entire system is given by

$$U = m_p g l(1 - \cos\theta) \tag{4}$$

Taking $q = (x,\ l,\ \theta)$ as the generalized coordinates corresponding to the generalized forces $f = (f_x, f_l,\ 0)$ and using Lagrange's equation

$$\frac{d}{dt}\left(\frac{\partial T}{\partial \dot{q}_i}\right) - \frac{\partial T}{\partial q_i} + \frac{\partial U}{\partial q_i} = f_i \tag{5}$$

for $i=1,2,3$. The equations of motion can be obtained as

$$\begin{gathered}(m_t + m_p)\ddot{x} + m_p\ddot{l}\sin\theta + m_p\, l\,\ddot{\theta}\cos\theta + 2\,m_p\,\dot{l}\,\dot{\theta}\cos\theta \\ -\, m_p\, l\,\dot{\theta}^2\sin\theta = f_x \\ m_p\ddot{x}\sin\theta + ((m_l + m_p)\ddot{l} - m_p\, l\,\dot{\theta}^2 - m_p\, g\cos\theta = f_l \\ \ddot{x}\cos\theta + l\ddot{\theta} + 2\,\dot{l}\,\dot{\theta} + g\sin\theta = 0\end{gathered} \tag{6}$$

The 3 DOF container crane system dynamics consists of two parts. The actuated dynamics, as described by the first two differential equation of (6) corresponds to the actuated states, the trolley position x and rope length l. The un-actuated dynamics, as given by the third differential equation of (6) corresponds to the un-actuated state, the payload swing angle θ. The un-actuated dynamics clearly shows the strong coupling between the states – trolley position x, rope length l and payload swing angle θ.

Among the assumptions taken, the trolley friction and wind disturbance are neglected. In the subsequent sections, the trolley friction and payload hoisting friction are modeled, initially in a simple way and later based on Lu-Gre friction model. In the subsequent section, the impact of wind load on the payload of container crane is also assessed.

A. Simple Friction Model

Friction is a natural phenomenon that occurs in any engineering systems involving motion and rotation. In cases where the effects of friction cannot be ignored, a good friction model is necessary for the design, control, and analysis of the system. The simple friction model of the container crane system, depicting the friction in trolley movement and cargo hoisting is given below:-

$$\text{Frictional force in trolley movement } F_t = b_t\,\dot{x}$$

$$\text{Frictional force in cargo hoisting } F_l = b_l\,\dot{l} \tag{7}$$

But this simple friction model cannot capture the complete frictional characteristics of a highly complex non linear container crane system. Among the various friction models, the Lu-Gre friction model captures the limit-cycle behavior and stick-slip oscillations effectively [12] and a brief discussion is given below.

B. LU-GRE Friction Model

Lu-Gre friction model was developed by Lund Institute of Technology, Sweden & University of Grenoble, France. Lu-Gre friction model can effectively incorporate the frictional behavior of complex nonlinear systems. A bristle interpretation of frictional interface is done in this model and the frictional force is measured in terms of Average bristle deflection, z [12]. Lu-Gre frictional force is given by

$$\begin{gathered}F = \sigma_0\, z + \sigma_1\,\dot{z} + \sigma_2\, v \\ \dot{z} = v - \sigma_0\,\frac{|v|}{|g(v)|}\,z \\ g(v) = \alpha_0 + \alpha_1\, e^{-(\frac{v}{v_s})^2}\end{gathered} \tag{8}$$

where v is the relative velocity between the two surfaces, z is the average bristle deflection, σ_0 is the aggregate bristle stiffness, σ_1 is the damping coefficient, σ_2 is the viscous friction coefficient, α_0, α_1 are static friction coefficients, v_S is a very small slip velocity, below which the frictional interface can be thought of as being "stuck".

The equations of motion for 3 DOF model of the container crane, including Lu-Gre frictional force in trolley movement and payload hoisting, can be obtained as

$$\begin{gathered}(m_t + m_p)\ddot{x} + m_p\ddot{l}\sin\theta + m_p\, l\,\ddot{\theta}\cos\theta + 2\,m_p\,\dot{l}\,\dot{\theta}\cos\theta \\ -\, m_p\, l\,\dot{\theta}^2\sin\theta = f_x - F_t \\ m_p\ddot{x}\sin\theta + ((m_l + m_p)\ddot{l} - m_p\, l\,\dot{\theta}^2 - m_p\, g\cos\theta \\ = f_l - F_l \\ \ddot{x}\cos\theta + l\ddot{\theta} + 2\,\dot{l}\,\dot{\theta} + g\sin\theta = 0\end{gathered} \tag{9}$$

Where F_t, the frictional force in trolley movement is given by

$$F_t = \sigma_0\, z + \sigma_1\,\dot{z} + \sigma_2\,\dot{x}$$

and F_l, Frictional force in cargo hoisting is given by

$$F_l = \sigma_0\, z + \sigma_1\,\dot{z} + \sigma_2\,\dot{l} \tag{10}$$

The dynamics of the container crane including Lu-Gre frictional force in trolley movement developed so far, can describe steady-state friction characteristics and supports hysteresis behavior due to frictional lag and spring-like behavior in stiction of the container crane.

C. Wind Load Assessment on the Payload of Container Crane

The container crane considered here is highly vulnerable to wind, as it is located on the seashore. The wind has two impacts on the container crane system – on its structure stability and on its payload. The structural stability of the container crane system is not in the scope of this paper. This section deals with the impact of wind on the payload of the container crane. The sway along the horizontal axis only is taken into consideration because it is the dominant component. The wind load [13] on the payload is given by

$$F_w = C_f A\, p_z$$

$$p_z = 0.6\, V_z^2$$

$$V_z = V_b\, K_1 K_2 K_3 \tag{11}$$

where C_f is the force coefficient in the direction of the wind for the payload structure, A is the effective frontal area of the part under consideration, in square metres, i.e. the solid area projection on to a plane perpendicular to the wind direction, p_z is the wind pressure corresponding to appropriate design condition in kiloNewtons per square metre, V_z is the design wind speed in m/s at any height z, V_b is the basic wind speed obtained from the wind speed map of the country, K_1 is the probability factor or risk co-efficient decided by the mean probable design life of structure in years and on the regional basic wind speed (its value is 1.0 for a design life of 50 years), K_2 is the factor decided by the terrain, height and size of the structure (its value is 1.05 for a Category-1 (open area/treeless plains) terrain and Class A (structure dimension less than 20m) structure size), K_3 is the topography factor.

The wind load on the payload of container crane can be modeled as an input disturbance in the form of a ramp signal or as a sinusoidal or as a random sequence. In this paper, an input wind disturbance of random sequence is applied to the 3 DOF model of the container crane, including Lu-Gre frictional force in trolley movement, given in equation (9).

V. Design Of Sliding Mode Controller

The container crane system container crane is unavoidably affected by uncertainties like changes in payload mass, rope length etc; and also by various kinds of disturbances such as the friction between the trolley and the rail, environmental factors like wind etc. So the essential need is for a robust control for uncertain systems. A general solution is Sliding Mode Control (SMC), which is a robust control technique, where the controller performance is guaranteed irrespective of parameter variations and external disturbances.

The 3 DOF container crane system contains three state variables that need to be controlled. The trolley position x and the rope length l are driven directly by control signals f_x and f_l, whereas the cargo swing θ is controlled indirectly and relies on the kinematic relationship between the actuated and un-actuated states. The objective is to design a control scheme to force the states x and l to converge to the desired values and for the payload swing angle θ to reach zero. The sliding surface can be defined as follows:

$$\begin{aligned} s &= [\, s_1 \quad s_2]^T \\ s_1 &= c_1 e_1 + c_2 e_2 + c_5 e_5 \\ s_2 &= c_3 e_3 + c_4 e_4 \end{aligned} \tag{12}$$

where *e (error) = state (x) - reference (r)*. e_1 corresponds to the error in trolley position, e_2 corresponds to the error in trolley velocity, e_3 corresponds to the error in rope length, e_4 corresponds to the error in rope velocity, e_5 corresponds to the error in swing angle and e_6 corresponds to the error in angular velocity. The references are given as [1 0 0.5 0 0 0]. The system dynamics given in equation (9) is rewritten in terms of error variables and c is designed by pole placement method, either by transformation approach [14] or by Ackermann's formula [15].

The control input is made up of two parts - u_c and u_{eq}. The control input u_c makes the system reach the sliding surface, u_c is taken as *-k*sign(s)*, where k is a high gain chosen. The control input u_{eq} is the equivalent control which makes the derivative of the sliding surface equal zero to stay on the sliding surface. It is obtained by substituting the derivative of the sliding surface equal to zero and find the corresponding u in terms of error dynamics as shown below. The control inputs are then obtained as follows:

$$\begin{aligned} u_1 = \; & m_p\, \dot{e}_4\, sine_5 + m_p\,(e_3 + r_3)\, \dot{e}_6\, cose_5 + \\ & 2m_p\,(e_3 + r_3) e_5\, cose_5 - m_p\,(e_3 + r_3)\, e_6{}^2\, sine_5 - \\ & (c_1 e_2 + c_5 e_6)(m_p + m_t) - k_1 * sign(s_1) \end{aligned}$$

$$\begin{aligned} u_2 = \; & -m_p\, \dot{e}_2\, sine_5 - m_p\,(e_3 + r_3)\, e_6{}^2 - m_p\, g\, cose_5 - \\ & c_3 e_4 (m_p + m_l) - k_2 * sign(s_2) \end{aligned} \tag{13}$$

The control input switches between two structures when s is close to zero, due to the sign function, which resulted in chattering, that causes high frequency oscillations of non-zero magnitude, which causes mechanical wear in the system and also actuates the un-modeled high frequency dynamics of system, thus deteriorating controller's performance. A solution to this chattering problem is a variable gain sliding mode controller, which is dealt in the next section.

In variable gain SMC, the control gain increases to high values until the sliding surface reaches the sliding mode, at which time the gain is switched to a low value to reduce chattering. The variable gain SMC customizes the gain k of the corrective control, u_c as follows:

if $|s| > \gamma > 0$, where γ is a small positive constant outside the chattering region, k is tuned as

$$k = \gamma \; |s| \tag{14}$$

where $\gamma > 0$ and $k > 0$. If $|s| \leq \varepsilon$, where ε is a small positive constant inside the chattering region, k is tuned as

$$k = \lambda \tag{15}$$

where λ is a meager positive constant and $k > 0$.

VI. Simulation Results

The system dynamics of 3 DOF model of onshore container crane system given by Eq.(9) when driven by the sliding mode control given in Eq. (13) has been simulated using MATLAB®. The system parameters used for the simulation are as follows:-

$m_t = 5$ kg, $m_l = 2$ kg, $m_p = 0.85$ kg, $g = 9.81 m/s^2$. The parameters of the controller are as follows: $c = [1.4 \quad 1 \quad 0.9 \quad 1 \quad 4]$ $k_1 = 2$, $k_2 = 5$. The initial trolley position $x(0) = 0$ m, initial rope length $l(0) = 0.2$ m and initial swing angle $\theta(0) = 0$.

The control input (13) should move the trolley to the destination 1 m, i.e. to $x(t_f) = 1$, payload is lowered to the desired rope length of 0.5 m i.e. $l(t_f) = 0.5$, by suppressing the cargo vibrations at the destination, i.e. $\theta(t_f) = 0$.

Fig. 3 shows the sliding surfaces, control input, trolley position, rope length and swing angle behavior of the sliding mode controlled 3 DOF model of onshore container crane system.

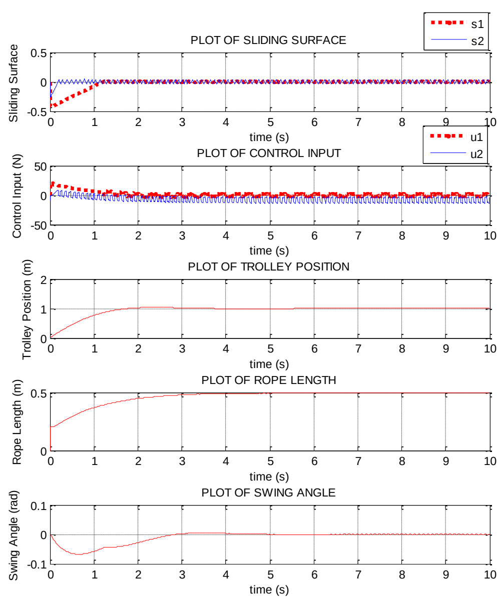

Fig 3. SMC Response of 3 DOF Container Crane Model

The sliding surfaces reached 0 within a considerably short time. The system responses asymptotically converged to the desired values after a relatively short time. It took 3 sec for the trolley position output to reach the desired value - 1m, with no overshoot. Cargo lowering motion reached 0.5 m in rope length after 3.5 s, with no overshoot. The payload swing angle was always kept small $|\theta_{max}| < 0.1$ radians during the transport process and it was completely eliminated at its destination after 4 s.

Fig. 4 shows the sliding surfaces, control input, trolley position, rope length and swing angle behavior of the sliding mode controlled 3 DOF model, when the payload mass is increased by 50 %.

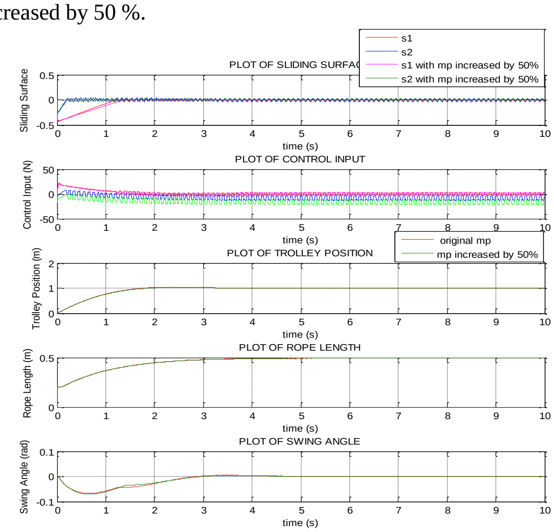

Fig 4. SMC Response of 3 DOF Model - Parameter Variation

The change in payload mass does not have an impact on the trolley position, rope length and the swing angle outputs. Thus sliding mode controller is robust even to 50% parameter variation. Fig. 5 shows the sliding surfaces, control input, trolley position, rope length and swing angle behavior of the sliding mode controlled 3 DOF model, when a random wind disturbance of standard deviation 0.01 is applied to the system throughout its operation.

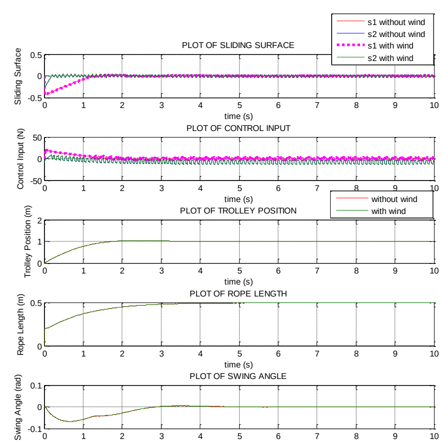

Fig.5. SMC Response of 3 DOF Model – Wind Disturbance

It is seen that the disturbance does not have an impact on the sliding surface and control input. The trolley position, rope length and the swing angle outputs are unaffected by the wind disturbance. It is noted that SMC is robust even to a disturbance applied after settling. It is also observed that the robustness is lost on increasing the magnitude of random disturbance (to a standard deviation 0.2) - the payload swing angle oscillate. Thus there is a limit for the sliding mode controller to withstand the disturbance. It can be judiciously used after evaluating the maximum level of disturbances that can occur in the system.

Fig. 6 shows the sliding surfaces, control input, trolley position, rope length and swing angle behavior of the variable gain sliding mode controlled 3 DOF model.

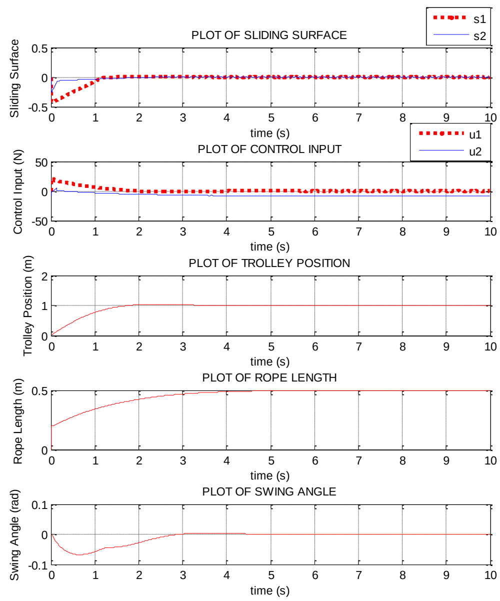

Fig 6. Variable Gain SMC Response of 3 DOF Model

As observed from the figure, the high frequency oscillations of non-zero magnitude that were existing in the control input with conventional SMC was completely eliminated in the variable gain approach. The system performance with conventional and variable gain SMC remains the same.

VII. CONCLUSION

Control of container cranes becomes necessary for automation of the transshipment terminals. This paper proposed a new 3 DOF model of the onshore container crane, including friction and wind disturbance, obtained using Lagrange equation. Sliding mode controller was applied with a sliding surface consisting of the trolley dynamics, hoisting dynamics and sway angle, to adjust with the uncertainties in the container crane system and reject the disturbances. A variable gain SMC is proposed as a new solution to solve the issue of chattering with conventional SMC and can be implemented practically, with the same system performance as with conventional SMC.

REFERENCES

[1] http://www.igtpl.com/

[2] Hahn Park, Dongkyoung Chwa, and Keum-Shik Hong, "A Feedback Linearization Control of Container Cranes:Varying Rope Length," International Journal of Control, Automation, and Systems, vol. 5, no. 4, pp. 379-387, August 2007.

[3] S. Garrido, M. Abderrahim, A. Gimnez, R. Diez, and C. Balaguer, "Anti-swinging input shaping control of an automatic construction crane," IEEE Trans. Autom. Sci. Eng., vol. 5, no. 3, pp. 549–557, Jul. 2008.

[4] B. Kimiaghalam, A. Homaifar, M. Bikdash, and G. Dozier, "Genetic algorithms solution for unconstrained optimal crane control," in Proc.Congr. Evolutionary Comput., 1999, vol. 3, pp. 2124–2130.

[5] Y. Fang, W. Dixon, D. Dawson, and E. Zergeroglu, "Nonlinear coupling control laws for an underactuated overhead crane system," IEEE/ ASME Trans. Mechatron., vol. 8, no. 3, pp. 418–423, Sep. 2003.

[6] M. Orbisaglia, G. Orlando, and S. Longhi, "A comparative analysis of sliding mode controllers for overhead cranes," in Proc. 16th Med. Conf. Control Autom., 2008, pp. 670–675.

[7] M. Park, D. Chwa, and S. Hong, "Antisway tracking control of overhead cranes with system uncertainty and actuator nonlinearity using an adaptive fuzzy sliding-mode control," IEEE Trans. Ind. Electron., vol. 55, no. 11, pp. 3972–3984, Nov. 2008.

[8] N. Sun, Y. Fang, Y. Zhang, and B. Ma, "A novel kinematic coupling based trajectory planning method for overhead cranes," IEEE/ASME Trans. Mechatron. vol. 17, no. 1, Feb. 2012.

[9] Q.H. Ngo K.-S. Hong, "Adaptive sliding mode control of container cranes," IET Control Theory Appl., 2012, Vol. 6, Iss. 5, pp. 662–668.

[10] Le Anh Tuan, Sang-Chan Moon, Won Gu Lee and Soon-Geul Lee, "Adaptive sliding mode control of overhead cranes with varying cable length," Journal of Mechanical Science and Technology 27 (3) (2013) 885-893.

[11] Le Anh Tuan, Soon-Geul Lee, Luong Cong Nho, and Dong Han Kim, "Model Reference Adaptive Sliding Mode Control for Three Dimensional Overhead Cranes," International Journal Of Precision Engineering And Manufacturing, Vol. 14, No. 8, pp. 1329-1338, August 2013.

[12] Nguyen B. Do, Aldo A. Ferri, Olivier A. Bauchau, "Efficient Simulation of a Dynamic System with LuGre Friction", Journal of Computational and Nonlinear Dynamics October 2007, Vol. 2 / 281.

[13] IS 14467 : 1997 IS0 4302 : 1981 Indian Standard Cranes -Wind Load Assessment , Bureau of Indian Standards

[14] V. I. Utkin and K.-K. D. Young, "Methods for constructing discontinuity planes in multidimensional variable structure systems," Automation and Remote Control, vol. 39, no. 10, pp. 1466–1470, 1978.

[15] Juergen Ackermann and Vadim Utkin, "Sliding Mode Control Design Based on Ackermann's Formula", IEEE Transactions on Automatic Control, Vol. 43, No. 2, February 1998.

SELF RECONFIGURABLE WIRELESS MESH NETWORKS UNDER DIFFERENT ROUTING PROTOCOLS

A. Sebin Sunny P , B. Ms. F Vincy Lloyd

***Abstract*—** WMN (Wireless Mesh network) is a communications network made up of radio nodes organized in a mesh topology. WMNs experience frequent link failures caused by channel interference, dynamic obstacles, or varying application's bandwidth demands. These failures cause severe performance degradation in WMNs or require expensive manual network management for their real-time recovery. Many solutions for WMNs to recover from wireless link failures have been proposed. But they have several limitations like global configuration changes, requirement of more network resources etc. Autonomous network reconfiguration system (ARS) is a technique that enables a multiradio WMN to autonomously recover from local link failures to preserve network performance. By using channel and radio diversities in WMNs, ARS generates necessary changes in local radio and channel assignments in order to recover from failures. Based on the generated configuration changes the system cooperatively reconfigure network settings among local mesh routers. ARS decouples network reconfiguration from flow assignment and routing. Reconfiguration might be able to achieve better performance if two problems are jointly considered. Simulation is done in Glomosim.

***Keywords*—** Wireless Mesh Network, Autonomous Reconfiguration System.

I. Introduction

Wireless Mesh Network (WMN) is a communications network made up of radio nodes organized in a mesh topology. Wireless mesh networks often consist of mesh clients, mesh routers and gateways. The mesh clients are often laptops, cell phones and other wireless devices while the mesh routers forward traffic to and from the gateways which may but need not connect to the Internet. The coverage area of the radio nodes working as a single network is sometimes called a mesh cloud. Access to this mesh cloud is dependent on the radio nodes working in harmony with each other to create a radio network. A mesh network is reliable and offers redundancy. When one node can no longer operate, the rest of the nodes can still communicate with each other, directly or through one or more intermediate nodes. Wireless mesh networks can be implemented with various wireless technology including 802.11, 802.16, cellular technologies or combinations of more than one type.

WMN may experience significant channel interference from other coexisting wireless networks. Some parts of networks might not be able to meet increasing bandwidth demands from new mobile users and applications. An autonomous network reconfiguration system (ARS) allows a multiradio WM to autonomously reconfigure its local network settings, channel, radio, and route assignment for real-time recovery from link failures, thus overcome the above mentioned limitations.

II. ARS ARCHITECTURE

ARS is a distributed system that is easily deployable in IEEE 802.11-based mr-WMNs. Running in every mesh node, ARS supports self-reconfigurability via the following distinct features:

• Localized reconfiguration: Based on multiple channels and radio associations available, ARS generates reconfiguration plans that allow for changes of network configurations only in the vicinity where link failures occurred while retaining configurations in areas remote from failure locations.

• QoS-aware planning: ARS effectively identifies QoS-satisfiable reconfiguration plans by: 1) estimating the QoS-satisfiability of generated reconfiguration plans; and 2) deriving their expected benefits in channel utilization.

• Autonomous reconfiguration via link-quality monitoring: ARS accurately monitors the quality of links of each node in a distributed manner. Furthermore, based on the measurements and given links' QoS constraints, ARS detects local link failures and autonomously initiates network reconfiguration.

• Cross-layer interaction: ARS actively interacts across the network and link layers for planning. This interaction enables ARS to include a rerouting for reconfiguration planning in addition to link layer reconfiguration.ARS can also maintain connectivity during recovery period with the help of a routing protocol.

ARS in every mesh node monitors the quality of its outgoing wireless links at every (e.g., 10 s) and reports the results to a gateway via a management message. Second, once it detects a link failure, ARS in the detector node triggers the formation of a group among local mesh routers that use a faulty channel, and one of the group members is elected as a leader using the well-known bully algorithm for coordinating the reconfiguration. Third, the leader node sends a planning request message to a gateway. Then, the gateway synchronizes the planning requests (if there are multiple requests) and generates a reconfiguration plan for the request. Fourth, the gateway sends a

Self Reconfigurable Wireless Mesh Networks Under Different Routing Protocols.

A. Author, Assistant Professor, Sreepathy Institute of Management And Technology, Palakkad, India-679533 .(phone: +91 9446870895; e-mail: sebinsunny@ simat.ac.in).

B. Author, Assistant Professor-ECE, Hindusthan College of Engineering and Technology, Coimbatore, India (e-mail: vincylloyd@gmail.com).

reconfiguration plan to the leader node and the group members. Finally, all nodes in the group execute the corresponding configuration changes, if any, and resolve the group. We assume that during the formation and reconfiguration, all messages are reliably delivered via a routing protocol and per-hop retransmission timer.

III. ROUTING PROTOCOLS

Given a source and destination node, a routing protocol provides one or more network paths over which packets can be routed to the destination. The routing protocol computes such paths to meet criteria such as minimum delay, maximum data rate, minimum path length etc. A routing metric that accurately captures quality of network links and thus aids in meeting such criteria is central to computation of good quality paths. The de- sign of routing metrics for wireless multi-hop networks is challenging due to following three unique characteristics of wireless links:

- Time varying channels and resulting variable packet loss:

The wireless links suffer from short term and long term fading and result in varying packet loss over different time scales. When the distance between the communicating nodes is large or if environment is obstacle rich and causes fading, the loss ratio of the link can be high. A routing metric should accurately capture this time varying packet loss.

- Packet transmission rate:

The packet transmission rate (or data rate) may vary depending upon the underlying physical layer technology. For example, 802.11a links have high data rate compared to 802.11b links. The data rate may also vary depending on the link loss characteristics when auto-rate control algorithms are used.

- Interference:

Wireless links operating in unlicensed spectrum suffer from two kinds of interference: (1) Uncontrolled interference results from non-cooperating entities external to the network that use the same frequency band but do not participate in the MAC protocol used by network nodes. For example, microwave ovens, Bluetooth devices operating in 2.4GHz ISM bands interfere with 802.11b/g networks in the same band. (2) Controlled interference: This kind of interference results from broadcast nature of wireless links where a transmission in one link in the network interferes with the transmissions in neighboring links. The interference of this kind depends on factors such as the topology of the network, traffic on neighboring links etc. It is well known that interference seriously affects the capacity of wireless networks in a multi-hop setting. It is important for a routing metric to capture the potential interference experienced by the links to find paths that suffer less interference and improve the overall network capacity. Interference can be either intra-path, wherein transmissions on different links in a path interfere or inter-path interference or inter-path wherein, transmissions on links in separate paths interfere. A more channel diverse multi-hop path has less intra-flow interference which increases the throughput along the path as more links can operate simultaneously if they operate on different orthogonal channels.

IV. RESULTS

The Simulation is carried out in Glomosim. Results obtained when different routing protocols are considered are shown below.

1. Bellmanford

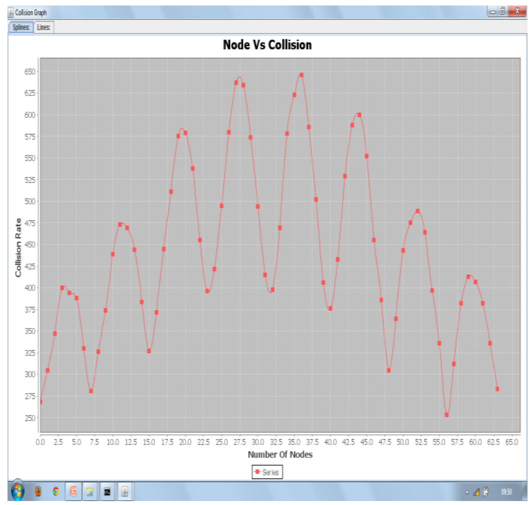

Fig 1. Node versus collision graph obtained for Bellmanford routing protocol.

2. AODV

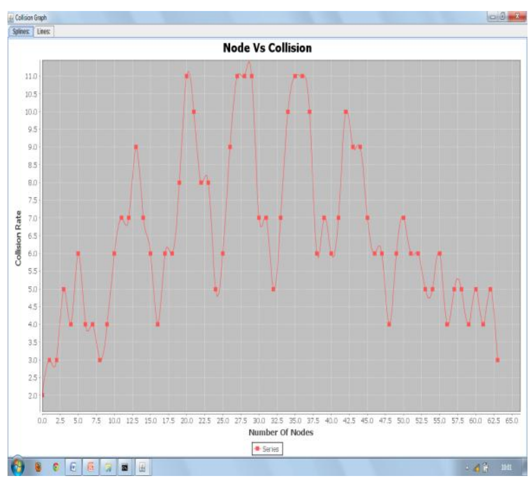

Fig 2. Node versus collision graph obtained for AODV routing protocol.

3.DSR

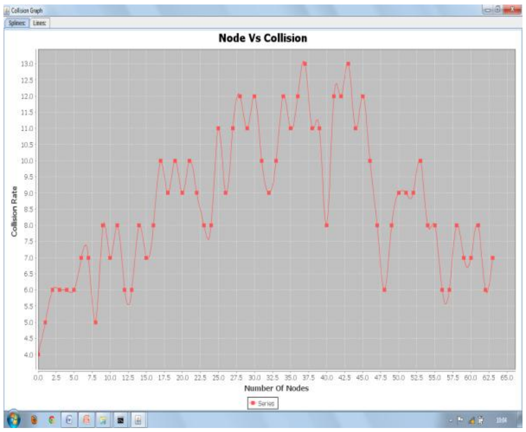

Fig 3. Node versus collision graph obtained for DSR routing protocol.

4.LAR

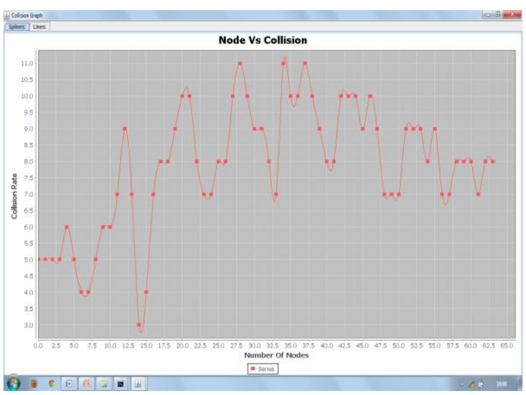

Fig 4. Node versus collision graph obtained for LAR routing protocol.

V. CONCLUSION

This paper evaluates the performance of ARS under different routing protocols using Glomosim. The results show that, different routing protocols have different effects on ARS. Also the results show that the ARS performance is increased when routing protocols are considered.

VI. FUTURE WORK

This paper proposes further research into more efficient protocols or variants of existing protocols. Also ARS decouples network reconfiguration from flow assignment and routing. Reconfiguration might be able to achieve better performance if two problems are jointly considered.

REFERENCES

[1] *Kyu-Han Kim, Kang G. Shin "Self-Reconfigurable Wireless Mesh Networks", IEEE/ACM transactions on networking, vol. 19, no. 2, April 2011*

[2] *I. Akyildiz, X. Wang, and W. Wang, "Wireless mesh networks: A survey," Comput. Netw., vol. 47, no. 4, pp. 445–487, Mar. 2005*

[3] *A. Akella, G. Judd, S. Seshan, and P. Steenkiste, "Self-management in chaotic wireless deployments," in Proc. ACM MobiCom, Cologne, Germany, Sep. 2005, pp. 185–199.*

[4] *P. Kyasanur and N. Vaidya, "Capacity of multi-channel wireless networks: Impact of number of channels and interfaces," in Proc. ACM MobiCom, Cologne, Germany, Aug. 2005, pp. 43–57.*

[5] *M. Alicherry, R. Bhatia, and L. Li, "Joint channel assignment and routing for throughput optimization in multi-radio wireless mesh networks," in Proc. ACM MobiCom, Cologne, Germany, Aug. 2005, pp. 58–72.*